J. Fluid Mech. (2020), *vol*. 899, A5. © The Author(s), 2020.
Published by Cambridge University Press
doi:10.1017/jfm.2020.424

Crest speeds of unsteady surface water waves

Francesco Fedele[1],†, Michael L. Banner[2] and Xavier Barthelemy[2,3]

[1]School of Civil and Environmental Engineering, Georgia Institute of Technology, Atlanta, GA 30332, USA

[2]School of Mathematics and Statistics, UNSW Australia, Sydney, NSW 2052, Australia

[3]Water Research Laboratory, School of Civil and Environmental Engineering, UNSW Australia, Sydney, NSW 2052, Australia

(Received 17 October 2019; revised 11 May 2020; accepted 22 May 2020)

Intuitively, crest speeds of water waves are assumed to match their phase speeds. However, this is generally not the case for natural waves within unsteady wave groups. This motivates our study, which presents new insights into the generic behaviour of crest speeds of linear to highly nonlinear unsteady waves. While our major focus is on gravity waves where a generic crest slowdown occurs cyclically, results for capillary-dominated waves are also discussed, for which crests cyclically speed up. This curious phenomenon arises when the theoretical constraint of steadiness is relaxed, allowing waves to change their form, or shape. In particular, a kinematic analysis of both simulated and observed open-ocean gravity waves reveals a forward-to-backward leaning cycle for each individual crest within a wave group. This is clearly manifest during the focusing of dominant wave groups essentially due to the dispersive nature of waves. It occurs routinely for focusing linear (vanishingly small steepness) wave groups, and it is enhanced as the wave spectrum broadens. It is found to be relatively insensitive to the degree of phase coherence and focusing of wave groups. The nonlinear nature of waves limits the crest slowdown. This reduces when gravity waves become less dispersive, either as they steepen or as they propagate over finite water depths. This is demonstrated by numerical simulations of the unsteady evolution of two- and three-dimensional dispersive gravity wave packets in both deep and intermediate water depths, and by open-ocean space–time measurements.

Key words: surface gravity waves

1. Introduction

Wind-generated ocean waves at the air–sea interface propagate predominantly in groups. Unsteady wave groups can exhibit a complex nonlinear life cycle, especially in focal zones where there is a rapid concentration of wave energy. Their structure and the associated carrier wave propagation depend on the dispersion, directionality and nonlinearity of waves, and their interplay. Understanding natural ocean wave propagation is not only of academic relevance, but it is also of importance in studying the energy exchange between wind and waves (Liberzon & Shemer 2011; Sullivan *et al.* 2018). Crest speeds are a key consideration for assessing the onset of breaking of a wave. In particular,

† Email address for correspondence: fedele@gatech.edu

https://doi.org/10.1017/jfm.2020.424 Published online by Cambridge University Press

Barthelemy *et al.* (2018) identified a new breaking onset threshold criterion based on energy flux considerations, which is valid for two-dimensional (2-D) and three-dimensional (3-D) wave groups in deep and intermediate water depths. While the energy flux that initiates breaking arises from energy focusing within the whole wave group, they found that the initial instability, or point of no return beyond which waves inevitably break, occurs within a very compact region centred on the maximum wave crest. Their new breaking criterion is based on the strength of the local energy flux relative to the local energy density, normalized by the local crest speed c. On the free surface, at the crest point, their dynamical criterion reduces to $B_x = u/c$, a kinematic condition for the ratio of crest fluid speed u to crest point speed c, where x is the direction of propagation. For maximally steep non-breaking waves, the crest fluid speed u cannot exceed 0.85 times the crest speed c, i.e. $B_x = 0.85$. In any event, their breaking onset threshold occurs well before the water speed outruns the crest speed.

In other applications, measurements of whitecap speeds have been proposed as a method for inferring ocean wavelengths (Phillips 1985), assuming that the Stokes dispersion relationship is applicable. Any systematic crest speed slowdown just prior to breaking onset can significantly alias wavelengths determined using the quadratic dispersion relation between Stokes wavelength and wave speed. Moreover, in the design of fixed and floating offshore structures, whitecap speeds are a key consideration in assessing wave impact loading on such structures, where flow-induced forces are proportional to the square of the water velocity. In particular, an $O(20\,\%)$ crest slowdown of breaking crests will result in an $O(50\,\%)$ reduction in their momentum flux loading. For non-breaking waves, crest slowdown effects will likely be much weaker.

The Stokes (1847) classical deep-water wave theory was developed for a steady, uniform train of 2-D nonlinear, deep-water waves of small-to-intermediate mean steepness ak $(= 2\pi a/L)$, where a is the wave amplitude and L is the wavelength. The phase speed c increases with ak as found to fifth order in wave steepness (see e.g. Fenton 1985):

$$c = c_0 \left(1 + \frac{1}{2}(ak)^2 + \frac{1}{8}(ak)^4 + O((ak)^6)\right), \tag{1.1}$$

where c_0 is the wave speed of linear (infinitesimally steep) waves.

The limiting phase speed of $1.1c_0$ for maximally steep steady waves follows by increasing the steepness up to the Stokes limit ($ak = \pi/7 \approx 0.449$). Increased wave steepness has long been associated with higher wave speeds. Historically, the Stokes theory has been the default theoretical approach for describing ocean waves (Wiegel 1964; Kinsman 1965). Contemporary studies by Beyá, Peirson & Banner (2012) found close agreement between monochromatic wave near-surface velocities and predictions based on fifth-order Stokes theory. Recent observational studies of velocities under extreme and breaking crests showed that inviscid predictions are in good agreement with particle image velocimetry-measured particle velocities (Grue *et al.* 2003). Further, Johannessen (2010) showed that at the crest of a non-breaking wave, near-surface velocities agree with second-order Stokes theory, which is capable of describing the free-surface kinematics very accurately provided that the local underlying regime of free waves can be identified. A principal constraint of the Stokes wavetrain framework is the imposed uniform spatial and temporal periodicity, which provides the basis for the extensive analytic treatment in the literature of this intrinsically nonlinear free-surface problem.

However, ocean waves propagate naturally in unsteady groups that evolve dynamically. Relaxing the periodicity constraints allows the manifestation of additional degrees of freedom, as reported in a number of laboratory and numerical wave tank studies. For

https://doi.org/10.1017/jfm.2020.424 Published online by Cambridge University Press

example, Melville (1983) found a phase speed variation of between $-17\,\%$ and $+32\,\%$ around the linear phase velocity. Shemer (2013) demonstrated that the crest propagation speed of dominant waves in broadbanded groups differs significantly from both their phase and group velocities. More specifically, crest slowdown phenomena have been observed for gravity waves and studied as a phase-resolved wave effect by several authors (Johannessen & Swan 2001, 2003; Johannessen 2010; Katsardi & Swan 2011; Shemer 2013; Shemer & Liberzon 2014; Shemer & Ee 2015). Deep-water breaking wave studies all found a significant $\sim O(20\,\%)$ breaking crest speed slowdown relative to the expected linear phase velocity (Rapp & Melville 1990; Melville & Matusov 2002; Melville, Veron & White 2002; Stansell & MacFarlane 2002; Jessup & Phadnis 2005).

Understanding gravity wave crest slowdown behaviour is central to the refining of the present knowledge of water-wave propagation and dynamics, and also to an effective implementation of Phillips' spectral framework for breaking waves (Phillips 1985; Gemmrich, Banner & Garrett 2008; Kleiss & Melville 2010). The groupiness of natural ocean gravity waves gives rise to a suite of differences from Stokes wave predictions. Baldock, Swan & Taylor (1996) report results of a laboratory study of an unsteady packet produced by an ensemble of unidirectional wave modes of different frequency components focusing in space and time. Subsequently, Johannessen & Swan (2001) extended that study to directional waves. Surface elevations and subsurface particle kinematics were compared with linear wave theory and the Longuet-Higgins & Stewart (1960) second-order solution of the wave–wave interactions. The study in Baldock *et al.* (1996) shows that nonlinear wave–wave interactions produce a highly nonlinear wave group with crests higher and troughs shallower than expected from numerical simulations by Longuet-Higgins (1987) and experiments by Miller, Shemdin & Longuet-Higgins (1991). Sutherland, Greated & Easson (1995) previously obtained very similar characterizations, although they also concluded that the wave kinematics were Stokes-like. Song & Banner (2002), Banner & Peirson (2007) and Viotti, Carbone & Dias (2014) report complementary numerical and experimental studies demonstrating that intra-group and inter-wave energy transfers cannot be neglected when characterizing wave group kinematics and dynamics.

Clearly, a Stokes characterization of waves has significant limitations when applied to fully nonlinear unsteady wave groups. Specifically, important properties derived from the Stokes (1847) theory and subsequent refinements by Fenton (1985) change fundamentally when stationarity is relaxed. Under gravity wave crest maxima, the velocity profiles differ systematically from those of a comparably steep Stokes wave. The unsteady leaning of waves (Tayfun 1986) is shown to be a critical aspect, determining the actual wave crest speed, now unsteady. In Banner *et al.* (2014), our preliminary numerical study of chirped wave groups provides an overview of the gravity wave crest slowdown phenomenon, and has already been verified against observations of wave groups in the laboratory and in the open ocean field (see also Fedele 2014*a*). This generic crest slowdown phenomenon has been recently observed by other researchers (Shemer & Liberzon 2014; Itay & Liberzon 2017; Khait & Shemer 2018; Craciunescu & Christou 2019*a*,*b*). It is investigated in much greater detail in the present paper.

2. Crest slowdown of linear gravity wave groups

Intuitively, crest speeds of water waves are assumed to match their phase speeds. However, our recent study highlights that this is generally not the case for natural water waves, which mostly occur in unsteady groups (Banner *et al.* 2014). Wave crest slowdown is observed as the manifestation of the natural dispersion of waves (Fedele 2014*a*). It arises when the theoretical constraint of steadiness is relaxed, allowing additional asymmetric

https://doi.org/10.1017/jfm.2020.424 Published online by Cambridge University Press

degrees of freedom in the wave motion. Generically, at focusing sites longer deep-water wave components overtaking shorter wave components reinforce to create a locally large wave. The crest of this wave undergoes a slowdown as it approaches its maximum amplitude, followed by a speedup during the subsequent decaying phase. We note that in strong contrast, in capillary wave packets, Fourier components with higher wavenumbers (shorter wavelengths) have larger phase speeds and overtake the slower-propagating longer capillary wave components. In this case, the crest speeds up as it attains its maximum amplitude, and then slows down. The wave crest height at focus depends on the packet amplitude spectrum (bandwidth and shape) and the degree of phase coherence during focusing. This occurs at a point when the tallest wave in group attains its maximum possible crest height by a constructive superposition of elementary harmonic waves, whose amplitudes depend upon the assumed spectrum. The full or partial coherence of their phases decides whether the focusing is perfect or imperfect, but the crest slowdown is practically insensitive to the degree of focusing, as discussed below. In the following, our study concentrates predominantly on gravity waves, but we will also consider waves in the capillary range for completeness.

2.1. *Perfect focusing*

Consider generic dispersive waves of a unidirectional Gaussian sea with frequency spectrum $E(\omega)$ and variance σ^2. The associated wavenumber spectrum $S(k) = E(\omega)(\mathrm{d}\omega/\mathrm{d}k)$, where $\omega(k)$ is the linear dispersion relation. Later, we will particularize our results to both deep and finite-depth water waves as well as capillary waves. A measure of the spectral bandwidth of the Gaussian sea can be defined as $\nu = \sqrt{m_0 m_2/m_1^2 - 1}$, where the spectral moments $m_j = \int \omega^j E(\omega)\,\mathrm{d}\omega$. The dominant wavenumber is k_0 and the associated frequency $\omega_0 = \omega(k_0)$.

Assume that a large crest of amplitude h is observed at $x = 0$ and $t = 0$. Boccotti (2000) showed that as $h/\sigma \to \infty$, the large crest belongs to a well-defined wave group that passes through $x = 0$ and it reaches its maximum focus at time $t = 0$. The surface displacement ζ of the group around focus is described, correct to $O(h^0)$, by the conditional random process (Fedele 2008; Fedele & Tayfun 2009):

$$\zeta(x,t) = \{\eta(x,t)|\eta(0,0) = h\} = h\left\{\Psi(x,t) + \Delta\frac{\Psi(x,t-T^*) - \psi^*\Psi(x,t)}{1-\psi^{*2}}\right\}, \quad (2.1)$$

where

$$\Psi(x,t) = \frac{\overline{\eta(\xi,\tau)\eta(\xi+x,\tau+t)}}{\sigma^2} = \int_0^\infty S_n(k)\cos(kx-\omega t)\,\mathrm{d}k \quad (2.2)$$

is the normalized space–time covariance of the surface elevation η and $S_n(k) = S(k)/\sigma^2$. The Boccotti parameter ψ^* is the first minimum of the time covariance $\psi(t) = \Psi(0,t)$ at $t = T^*$. Physically, ζ represents a dispersive broadbanded linear (small steepness) wave group, with no restriction on the spectral bandwidth. The largest crest occurs at the apex of the group as a result of a constructive interference, that is, the phases of its elementary Fourier components become perfectly coherent. Given a large crest amplitude $h \gg \sigma$, Fedele & Tayfun (2009) showed that the dimensionless residual Δ is Gaussian distributed with zero mean and standard deviation $\sigma_\Delta = \sqrt{1-\psi^{*2}}\sigma/h$. As h becomes larger, σ_Δ tends

https://doi.org/10.1017/jfm.2020.424 Published online by Cambridge University Press

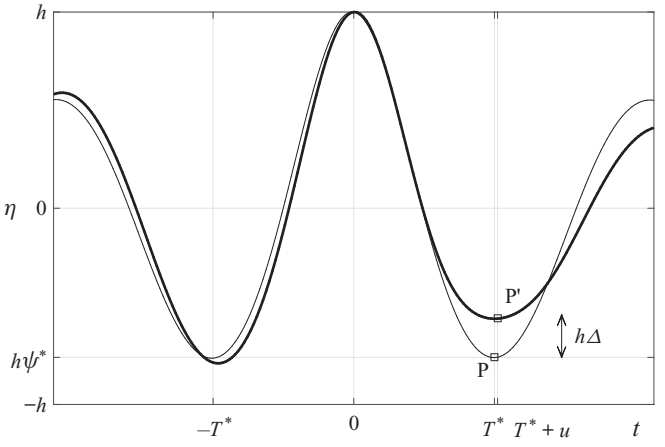


FIGURE 1. Time profile $\zeta(x=0,t)$ of the stochastic wave group of (2.1) at the focusing point ($x=0$). The thin line is the scaled covariance function $h\psi(t)$, which represents the symmetric wave profile of a crest in the limit of infinite amplitude $h/\sigma \to \infty$. The crest is followed by a trough at $T=T^*$ (point P) and amplitude $\eta_{tr}=h\psi^*$. The preceding trough occurs at $t=-T^*$ because of symmetry of $\psi(t)$. For finite but large crest amplitudes ($h/\sigma \gg 1$), the wave profile is depicted by the bold line. The trough now occurs at $t=T^*+u$ (point P′) with u of $O(h^{-1})$ (negligible to $O(h^0)$; see Fedele & Tayfun (2009)) and the amplitude $\eta_{tr}=h(\psi^*+\Delta)$, with $h\Delta$ of $O(h^0)$ (Fedele & Tayfun 2009). Note that for $\Delta \neq 0$ the symmetry of the wave profile (bold line) is broken.

to zero and Δ tends to a deterministic variable in the limit of infinite height (Boccotti 2000; Fedele & Tayfun 2009).

In our simulations, we sample from the population of wave groups with $\sigma_\Delta \approx 0.1$–$0.2$ and sample values of Δ in $\pm\sigma_\Delta$. The large crest at $t=0$ is followed by a trough at $t=T^*+u$, with u negligible as of $O(h^{-1})$ (Fedele & Tayfun 2009). From (2.1), the trough amplitude is $h_{tr}=h(\psi^*+\Delta)$, where $\psi^*<0$ (see figure 1).

The parameter Δ measures the asymmetry of the wave profile. In particular, the wave group (2.1) attains the given crest height h at the focal point ($x=0, t=0$), irrespective of Δ, by way of a constructive interference of elementary waves. When $\Delta=0$, the phase coherence is perfect as the evolution of the wave group is perfectly symmetric before and after focus (see thin line in figure 1). Clearly, the probability of such perfectly symmetric occurrences ($\Delta=0$) is null as it occurs in the limit of infinite crest heights (Boccotti 2000; Fedele & Tayfun 2009). For a finite and large amplitude h, $\Delta \neq 0$ breaks the symmetry of the stochastic wave group kinematics (see bold line in figure 1). This introduces hysteresis as explained below.

The crest speed c of the tallest crest of the stochastic wave group in (2.1), where $\partial_x\zeta=0$, is given by (Longuet-Higgins 1957)

$$c=-\frac{\partial_{xt}\zeta}{\partial_{xx}\zeta}, \tag{2.3}$$

which is also valid for nonlinear surfaces. Stationarity is attained at the focusing point and the associated speed value c_s of c is given by the weighted average of the linear phase

https://doi.org/10.1017/jfm.2020.424 Published online by Cambridge University Press

speed $C(k) = \omega(k)/k$ of Fourier waves as (Fedele 2014*a*,*b*)

$$c_s = \frac{\int S(k)k^2 C(k)\,\mathrm{d}k}{\int S(k)k^2\,\mathrm{d}k} + O(h^{-1}). \tag{2.4}$$

For spectra with narrow bandwidth ($\nu \ll 1$),

$$c_s = c_0 + \left[2k_0 C'(k_0) + \frac{1}{2}k_0^2 C''(k_0)\right]\nu^2 + o(\nu^2), \tag{2.5}$$

where $c_0 = C(k_0)$ is the linear phase speed at the spectral peak $k = k_0$, and $C'(k_0)$ and $C''(k_0)$ are the derivatives of $C(k)$ with respect to the wavenumber k evaluated at the same spectral peak.

Moreover, from (2.4), following the crest path where $\partial_x \eta = 0$ (Fedele 2014*a*), the time-varying crest speed $c(t)$ can be Taylor-expanded around the focusing time $t = 0$ near the crest maximum

$$c = c_s + \frac{1}{2}\ddot{c}(0)t^2 + O(t^4), \tag{2.6}$$

and the time curvature at $t = 0$ follows by taking the second derivative of (2.3) with respect to time

$$\ddot{c}(0) = -\frac{c_s^3}{\partial_{xx}\zeta}\mathcal{L}(\partial_x \zeta), \tag{2.7}$$

where the differential operator

$$\mathcal{L} = \left(\partial_x + \frac{1}{c_s}\partial_t\right)^3. \tag{2.8}$$

In spectral form

$$\ddot{c}(0) = c_s^3 \frac{\int k^4 \left(1 - \dfrac{C(k)}{c_s}\right)^3 S(k)\,\mathrm{d}k}{\int k^2 S(k)\,\mathrm{d}k}. \tag{2.9}$$

The sign of the time curvature $\ddot{c}(0)$ determines the tendency of the crest to slow down or speed up as the focal point is reached. In particular,

$$\ddot{c}(0) = 6k_0^2 C'(k_0)^3 \nu^2 + o(\nu^2). \tag{2.10}$$

For linear dispersive waves with $\omega(k) \sim k^n$, $C(k) \sim k^{n-1}$ and $C'(k_0) = (n-1)k_0^{n-2}$. Thus, crests slow down in the deep-water wave regime since $n = 1/2 < 1$. On the contrary, crests speed up in the capillary wave regime, for which $n = 3/2 > 1$. Moreover, the slowdown/speedup is of $O(\nu^2)$. Thus, it arises with the modulation of the wave group and it increases as the spectrum becomes more broadbanded, as ν increases.

We note in passing that the above formalism and analysis for unidirectional (2-D) wave groups are easily extendable to multidirectional (3-D) wave packets drawing on Fedele &

https://doi.org/10.1017/jfm.2020.424 Published online by Cambridge University Press

Tayfun (2009). In particular, consider a polar frame (k, θ) and the dominant direction of waves along x, or $\theta = 0$. Then, the crest speed c_s in (2.4) extends to 3-D groups as

$$c_{s,3D} = \frac{\iint S(k,\theta)\,\omega(k)k\,\cos\theta\,\mathrm{d}k\,\mathrm{d}\theta}{\iint S(k,\theta)k^2\cos^2\theta\,\mathrm{d}k\,\mathrm{d}\theta} + O(h^{-1}), \tag{2.11}$$

where $S(k, \theta)$ is the directional wave spectrum. Drawing on Fedele (2015), consider narrowband waves with spectral bandwidth ν and directional spreading σ_θ around the dominant wave direction $\theta = 0$. Then,

$$c_{s,3D} = c_{s,2D}\left(1 + \frac{\sigma_\theta^2}{2}\right) + O(\sigma_\theta^4). \tag{2.12}$$

Clearly, the crest slowdown of 3-D wave groups manifests similar trends and properties as those of 2-D wave groups, with a mild influence by the directional structure of the group.

In summary, our analysis reveals that the crest slowdown effect in dispersive gravity-dominated waves can be very significant even during linear wave-focusing events, provided that the spectral bandwidth is sufficiently large. On the other hand, crest slowdown reduces as crests propagate over shallower waters, because waves tend to be less dispersive. In sharp contrast, crests of dispersive capillary-dominated waves tend to speed up. Finally, the crest slowdown of 3-D wave groups has behaviour similar to that of 2-D groups, as also clearly illustrated below by our results drawn from open-ocean space–time data (see figure 10).

2.2. *Crest slowdown of deep-water gravity waves*

Consider a unidirectional sea state of deep-water gravity waves with linear dispersion $\omega^2 = gk$ and g the gravity constant. The sea spectrum has a broad range of spectral frequencies (bandwidth $\nu \approx 0.5$) and the conventional JONSWAP form. In particular, a peak enhancement parameter $\gamma = 3.3$ and spectral decay $E(\omega) \sim \omega^{-5}$ or $S(k) \sim k^{-3}$, characteristic of realistic ocean waves (Hasselmann *et al.* 1973; Komen 1994). We note in passing that our results and conclusions are the same for a Kolmogorov–Zakharov spectral decay $E(\omega) \sim \omega^{-4}$ (Zakharov 1968, 1999). We also assume a perfect (symmetric) focusing of the stochastic wave group in (2.1), i.e. $\Delta = 0$. Equation (2.1) is solved numerically by standard Fourier methods ($N \sim 10^4$ modes) on a computational domain long enough ($O(50)$ dominant wavelenghs L_0) to ensure zero-boundary conditions. The wave packets are localized in space and never reach the boundaries during the one-time focusing event.

Figure 2(*a*) depicts the time stack of the simulated surface profile η as waves propagate from left to right. Significant leaning and slowdown are observed around a point of maximum crest height. In particular, the tallest wave crest of the group leans forward (A) prior to approaching the maximum of the group at the focusing site (B). At this stage, the crest has a steeper front face than its rear face, suggesting that it should accelerate as it approaches the focusing site and then eventually break. That would be the case if the wave were not able to continue to grow in amplitude. On the contrary, it is seen that the forward-leaning wave relaxes at (A) to a symmetric shape as it accumulates potential energy reaching its tallest height at (B). While doing so, the wave crest decelerates significantly by $O(30\,\%)$, as it attains its maximum height at (B). Since the process is linear, with perfect constructive interference, the reverse of the wave growth phase

https://doi.org/10.1017/jfm.2020.424 Published online by Cambridge University Press

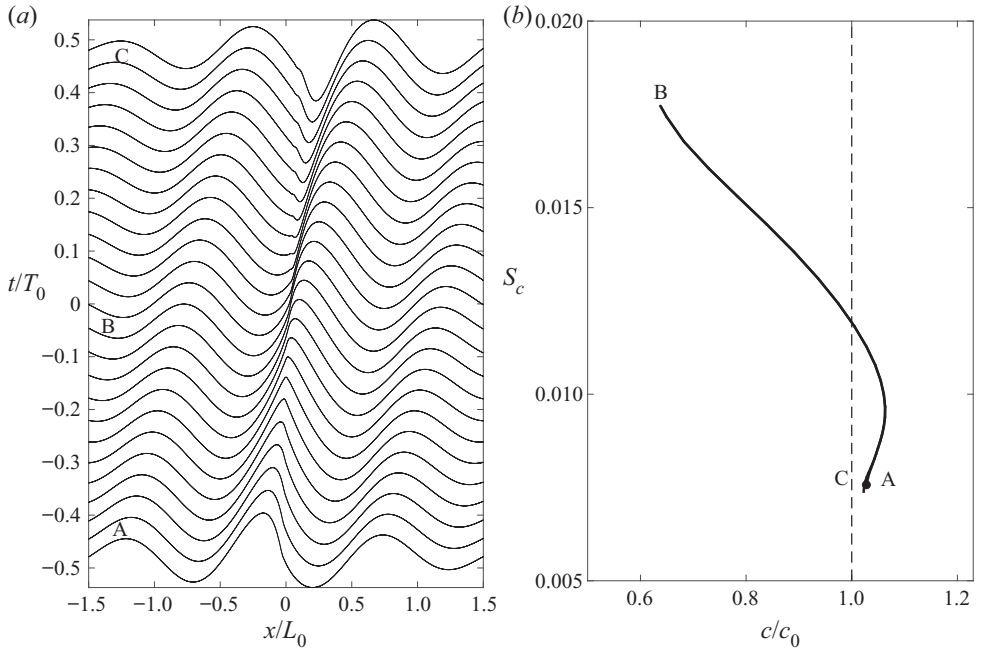


FIGURE 2. Perfect focusing of a deterministic linear broadband gravity wave group in deep water (JONSWAP spectrum, spectral bandwidth $\nu \approx 0.5$). (*a*) Time stack of the surface profile ζ as waves propagate from left to right. Before focus (A), the crest leans forward as it slows down reaching the largest height at focus (B) and then leans backward while accelerating after focus (C). Note that the smaller adjacent crests undergo a similar evolution. (*b*) Hysteresis curve of the normalized crest speed c/c_0 (bold line) of the tallest wave as a function of the local crest steepness S_c. The Stokes theory predicts the crest speed $c/c_0 = 1$, as shown by the dashed vertical line. Here, as defined in § 2.2, c_0 is the reference linear deep-water phase speed of the dominant frequency ω_0. The leaning cycle has a duration close to the dominant period $T_0 = 2\pi/\omega_0$.

commences and it is exactly symmetric with the earlier growing phase. After focus, the wave crest leans backwards at (C) and the rear face of the wave crest is now steeper than its front face. This suggests that the crest should now decelerate as it travels away from the focusing site. On the contrary, the backward-leaning wave crest face (C) accelerates while it reduces in amplitude, releasing the accumulated potential energy to the wave group.

Note that the smaller adjacent crests undergo similar evolution. We observe that the leaning cycle has a duration close to the dominant wave period $T_0 = 2\pi/\omega_0$ irrespective of the spectral bandwidth. This is reasonable since all the waves in a group, irrespective of its length, undergo the same cyclical crest slowdown as also observed in our nonlinear numerical simulations shown below.

Crest slowdown is more evident in figure 2(*b*), which depicts the normalized crest speed c/c_0 of the tallest wave as a function of its local crest steepness $S_c = k_c a_c$. Here, a_c is the amplitude of the crest and $k_c = 2\pi/L_c$ is the associated local wavenumber, with L_c being the distance between the two zero-crossings before and after the crest. The reference $c_0 = \omega_0/k_0$ is the phase speed at the dominant frequency ω_0. Note that the Stokes theory predicts the crest speed $c/c_0 = 1$, as shown by the dashed vertical line. Since the focusing is perfect, there is no hysteresis in the plot of c/c_0 versus S_c, since

https://doi.org/10.1017/jfm.2020.424 Published online by Cambridge University Press

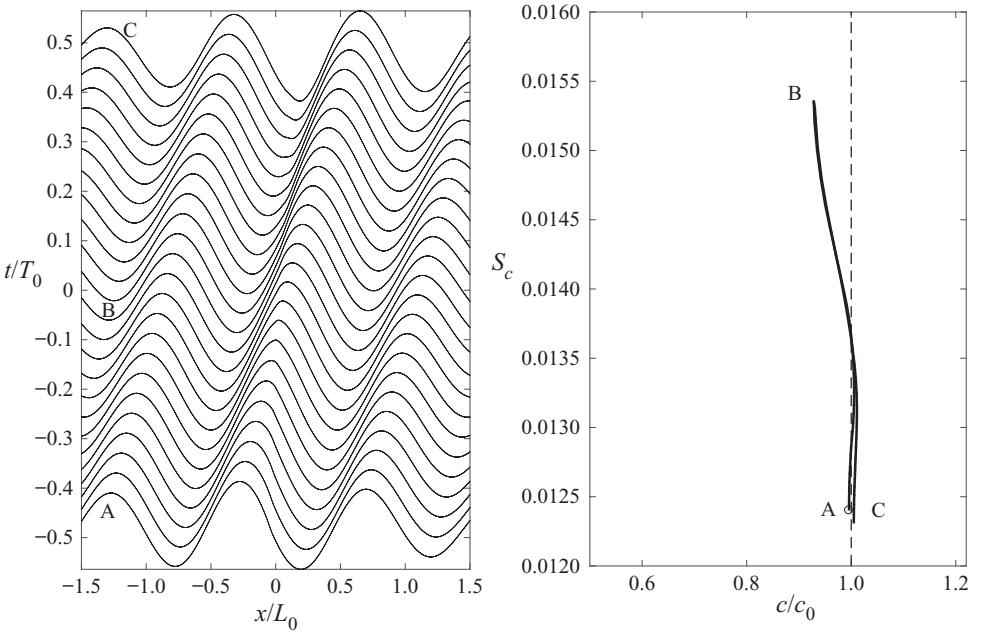


FIGURE 3. Focusing of the deterministic linear narrowband wave group in deep waters (JONSWAP spectrum, spectral bandwidth $\nu \approx 0.1$). Other symbols are as in caption of figure 2.

the growing and decaying phases of the group are symmetric. We point out that both the vertically integrated potential and kinetic energy densities following the crest of the tallest wave increase as the crest slows down, with potential energy density growing more than kinetic energy density since potential energy density accumulates around the growing crest (Barthelemy *et al.* 2018). Clearly, this is due to the linear nature of the wave group. Nonlinearities suppress the growth of potential energy while favouring that of the kinetic energy as a precursor to breaking.

On the contrary, the same JONSWAP wave group with a narrowband spectrum ($\nu \approx 0.1$) manifests a very mild crest slowdown and the changing shape of the crest form due to leaning is barely noticeable. This is clearly seen in figure 3. The life cycle of the crest is still symmetric and there is no hysteresis.

Clearly, the probability of such perfectly symmetric occurrences ($\Delta = 0$) is null as it occurs in the limit of infinite crest heights (Boccotti 2000; Fedele & Tayfun 2009). For finite and large amplitude h, the effects of the parameter Δ on kinematics of the stochastic wave group ζ and associated crest slowdown and leaning cycle are shown in figure 4. Here, we see that the crest height is unchanged and we only observe variations in the leaning cycle that affect the crest slowdown. In particular, the slowdown increases as the crest tends to lean more backward (thin line, $\Delta > 0$) in comparison with the symmetric case (bold line, $\Delta = 0$). On the contrary, the slowdown reduces as the crest leans less backward (dash-dotted line, $\Delta < 0$). Moreover, the symmetry around focus is broken as clearly seen in figure 4 from the diagrams of the crest speed c/c_0 versus the local crest steepness S_c. The curves enclose a finite area, which is a measure of the deviation from the ideal symmetry that characterizes perfect focusing.

https://doi.org/10.1017/jfm.2020.424 Published online by Cambridge University Press

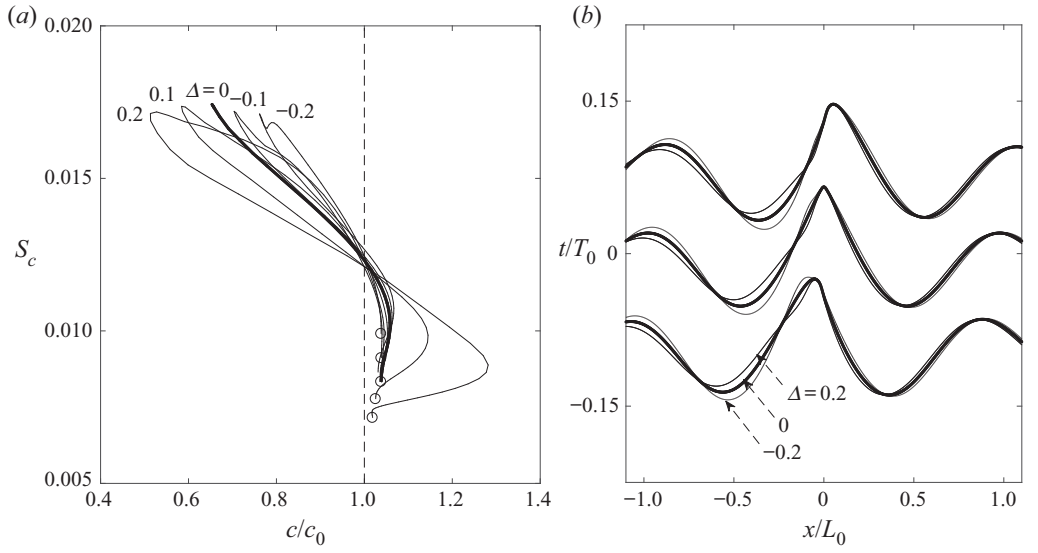


FIGURE 4. Linear crest slowdown and leaning cycle of a focusing gravity wave group in deep water (JONSWAP spectrum, spectral bandwidth $\nu = 0.4$). (*a*) Hysteresis curve of the normalized crest speed c/c_0 of the tallest wave as a function of its local crest steepness S_c for different values of the parameter Δ. Here, c_0 is the reference linear deep-water phase speed of the dominant frequency ω_0. The linear Stokes theory predicts the crest speed $c/c_0 = 1$, as shown by the dashed vertical line. (*b*) Time stack of the surface profile ζ as waves propagate from left to right for three different values of Δ, i.e. -0.2, 0 and 0.2. The leaning cycle has a duration close to the dominant period T_0. The crest leans forward as it slows down reaching the largest height at focus and then leans backward while accelerating.

2.3. *Crest slowdown of gravity waves in intermediate-depth water*

Consider a synthesized sea state of gravity waves propagating in waters of depth d and linear dispersion relation $\omega^2 = gk\tanh(kd)$. For simplicity we assume a JONSWAP spectrum for the evolution of the stochastic wave group in (2.1), and parameters $\nu = 0.3$, $\Delta = 0.2$. Our results and conclusions are qualitatively the same for a Gaussian-shape spectrum. Figure 5(*a*) depicts the hysteresis curves of the normalized crest speed c/c_0 of the tallest wave as a function of its local crest steepness S_c for three values of water depth $d/L_0 = 0.05, 0.1, \infty$. Here, we recall that c_0 is the linear phase speed for the depth d/L_0 and the spectral peak frequency $\omega_0 = 2\pi/T_0$, with L_0 the associated wavelength.

When the tallest wave of the group propagates over shallower water depths its local crest steepness S_c increases, but the hysteresis cycles shift to the right and the relative slowdown within the cycle is also reduced. This reduction is associated with the fact that waves lean less when they propagate over shallower water depths, as clearly seen in figure 5(*b*). In sharp contrast, in the following we will show that crests speed up in the capillary wave regime.

2.4. *Crest speedup in the capillary regime*

Consider now the evolution of the stochastic wave group ζ in (2.1) with capillary dispersion $\omega(k) \sim k^{3/2}$, and spectrum $E(\omega) \sim \omega^{-2.5}$, or $S(k) \sim k^{-3.25}$. We also set $\Delta = 0.2$. Figure 6(*a*) depicts the time stack of the surface profile ζ as waves propagate from

https://doi.org/10.1017/jfm.2020.424 Published online by Cambridge University Press

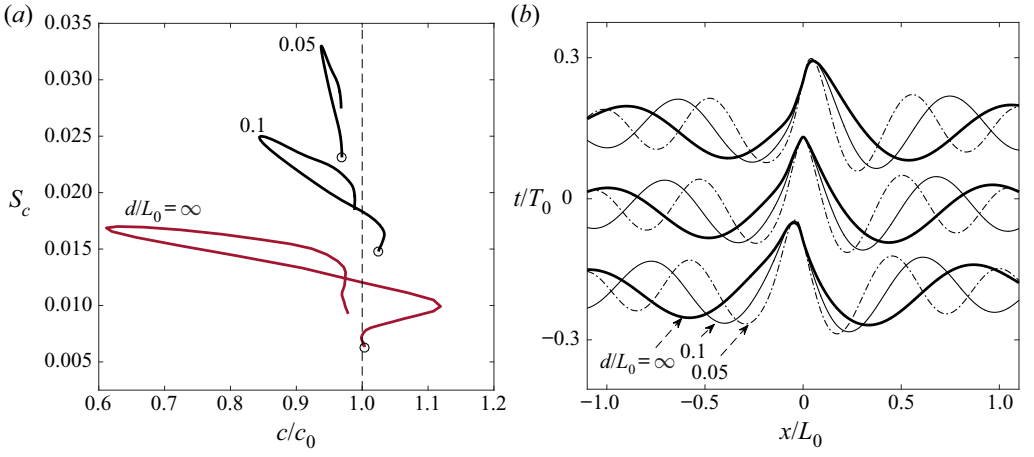


FIGURE 5. Water depth effects on the linear crest slowdown and leaning cycle of a stochastic wave group (JONSWAP spectrum, spectral bandwidth $\nu = 0.3$, $\Delta = 0.2$). (*a*) Hysteresis curve of the normalized crest speed c/c_0 of the tallest wave as a function of the local steepness S_c for different values of the water depth $d/L_0 = 0.05, 0.1, \infty$. Here, c_0 is the linear phase speed at the finite depth d/L_0 and at spectral peak $\omega_0 = 2\pi/T_0$, with L_0 the associated wavelength. (*b*) Time stack of the surface profile η_c as waves propagate from left to right for the three values of d/L_0.

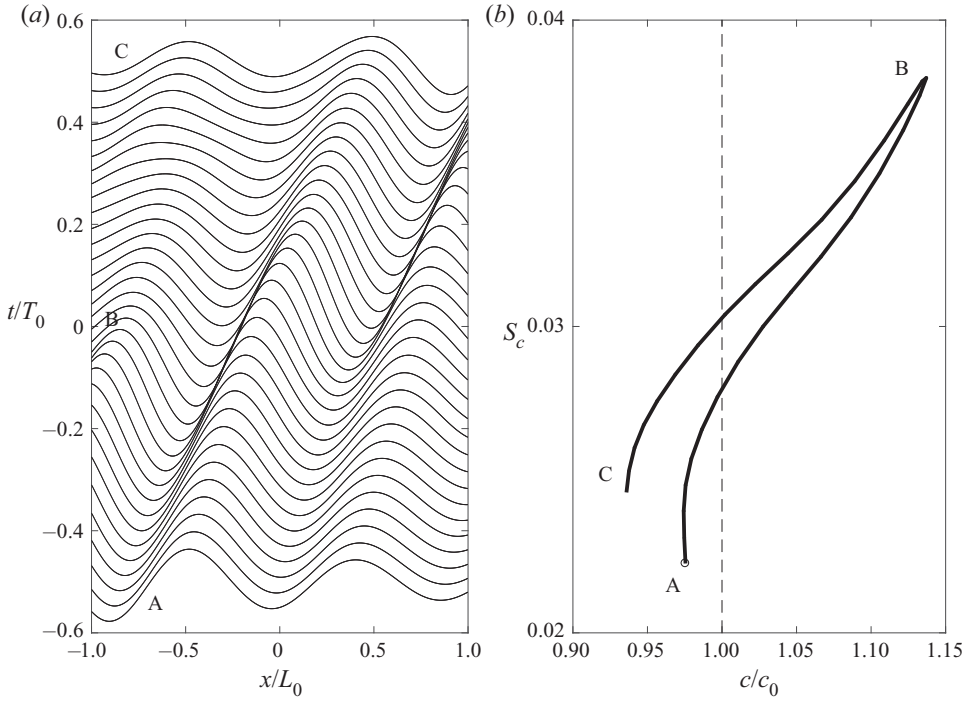


FIGURE 6. Capillary waves: focusing of a stochastic wave group. Here, c_0 is the reference linear phase speed of the dominant frequency ω_0. Other symbols are as in the caption of figure 2.

https://doi.org/10.1017/jfm.2020.424 Published online by Cambridge University Press

left to right. In particular, the tallest wave crest of the group leans backward (A) prior to approaching the maximum of the group at the focusing site (B). At this stage, the crest has a gentler sloping front face than its rear face. The rearward-leaning wave at (A) relaxes to a symmetric shape as it accumulates potential energy reaching its tallest height at (B). While doing so, the wave crest accelerates significantly as it grows in amplitude, attaining its maximum height at (B). Then, the reverse of the wave growth phase commences. In particular, after focus the wave crest then leans forward (C) and the forward face of the wave is now steeper than its rear face. The forward-leaning wave crest (C) decelerates while it reduces in amplitude, releasing the accumulated potential energy to the wave group. The leaning cycle has a duration close to the dominant wave period T_0. The crest speedup can be clearly observed in figure 6(b), which depicts the hysteresis diagram of c/c_0 versus S_c. The speedup is more pronounced as the energy of shorter capillary waves becomes comparable to that of longer waves. This is because shorter capillary waves travel faster than longer waves. For instance, the speedup is practically unnoticeable if the spectrum $E(\omega)$ decays as fast as ω^{-5}, or $S(k) \sim k^{-7}$.

In the following, we will study the effect of imperfect focusing on the crest slowdown. The maximum crest height is clearly affected, but we will show that the crest slowdown is practically insensitive to the degree of phase coherence of a group. Thus, crest slowdown is purely an effect of the natural dispersion of waves. In particular, the crest slowdown and associated leaning reduces as the dispersion is reduced when linear waves travel over shallower water depth. In the following, we will show that this is a generic property of the crest slowdown. Moreover, even nonlinearities affect the slowdown of crests because waves become less dispersive as they steepen.

2.5. *Imperfect focusing*

Consider a linear wave group whose elementary Fourier components have phases not perfectly coherent. Drawing on Latifah & van Groesen (2012), the associated surface displacements can be described by (Fedele 2008; Fedele & Tayfun 2009)

$$\zeta(x,t;\alpha) = h\int_0^\infty S_n(k)\cos(kx-\omega(k)t+\alpha\theta(k))\,\mathrm{d}k. \tag{2.13}$$

When $\alpha = 0$ (perfect coherence), the maximum crest height h is attained at focus. The degree of phase coherence is measured by the defocusing factor α (Latifah & van Groesen 2012) and $\theta(k)$ is a random phase function of k. In particular, at any k, the phase θ is a uniform random variable distributed in $[-\pi,\pi]$ with mean $\mu(k) = 0$ and standard deviation $\sigma(k) = \pi/\sqrt{3} \approx 0.58\pi$. A set of N phases $\theta_j = \theta(k_j)$ at different wavenumbers k_j are stochastically independent and their joint probability density function is

$$p(\theta_1,\theta_2,\ldots,\theta_N) = \frac{1}{(2\pi)^N}. \tag{2.14}$$

Note that this is one of the ways to model the imperfect phase coherence of a wave group. A first look at ζ in (2.13) suggests that it is a random process. On the contrary, ζ is deterministic as a result of the strong law of large numbers. Therefore, it assumes the form (see appendix A)

$$\zeta(x,t;\alpha) = \widetilde{h}(\alpha)\int S_n(k)\cos(kx-\omega t)\,\mathrm{d}k. \tag{2.15}$$

https://doi.org/10.1017/jfm.2020.424 Published online by Cambridge University Press

This is identical to a perfectly focusing packet $\zeta(x,t;\alpha=0)$ in (2.1), except that now its crest amplitude is smaller than the maximal height h as a consequence of phase decoherence, that is

$$\widetilde{h}(\alpha)=h\frac{\sin(\pi\alpha)}{\pi\alpha}. \tag{2.16}$$

Nevertheless, the crest of the defocused wave group ($\alpha\neq 0$) still experiences the same amount of linear slowdown and leaning as that of a perfectly focused wave group ($\alpha=0$), because the shape of the packet is unchanged, that is

$$\frac{\zeta(x,t;\alpha)}{\widetilde{h}(\alpha)}=\frac{\zeta(x,t;0)}{\widetilde{h}(0)}. \tag{2.17}$$

As a result, from (2.3)

$$c(\alpha)=-\frac{\partial_{xt}\zeta(x,t;\alpha)}{\partial_{xx}\zeta(x,t;\alpha)}, \tag{2.18}$$

and, with probability 1, the minimum crest speed

$$c_s(\alpha)=c_s(0), \tag{2.19}$$

implying that an imperfectly focused wave crest slows down as much as a perfectly focused wave crest, and the speed c_s is given in (2.4). In passing, we point out that 3-D wave groups have similar behaviour.

In summary, the crest slowdown of linear gravity wave groups is insensitive to the degree of phase coherence of the wave group. The associated leaning cycle is purely the effect of the natural dispersion of waves as discussed later on. Note also that nonlinear effects on the crest slowdown are attenuated since the wave amplitude is reduced.

3. Geometry and nonlinearities

Geometric changes of each individual wave inside the packet are strongly phase-locked as seen, for example, in figure 7. Each wave leans forward following its creation at the rear of the packet, becomes symmetric as it reaches the crest maximum at focus and then leans backward as it disappears at the front of the packet. The leaning or asymmetry of the evolving shape of a focused crest is purely a linear phenomenon due to the dispersive nature of water waves, and it can be explained in terms of geometric phases (Fedele 2014*a*).

The forward leaning of the wave before focus (sharper front and gentler back) is the kinematic manifestation of the longer wave components being behind the shorter ones. As focus is attained, longer waves catch up with the shorter ones. As a result, the wave accumulates potential energy as it slows down and the crest amplitude increases. At focus, the profile becomes symmetric and the crest attains its maximal height as the potential energy growth is zero. After focus, the wave crest accelerates while it reduces its amplitude, releasing potential energy to the wave group. The longer waves are now ahead of the shorter ones and the wave leans backward (sharper back and gentler front). Thus, the leaning of crests is the kinematic manifestation of linear dispersive focusing.

According to Fedele (2014*a*), the crest slowdown phenomenon, which manifests when unsteadiness plays a role in the wave group propagation, has its theoretical origin in the geometric phase framework in quantum mechanics (e.g. Berry 1988; Wilczek & Shapere 1989). Only recently has it been investigated in detail for unsteady deep-water wave packets (Fedele 2014*a*). The forward leaning and subsequent crest slowdown are primarily linear

https://doi.org/10.1017/jfm.2020.424 Published online by Cambridge University Press

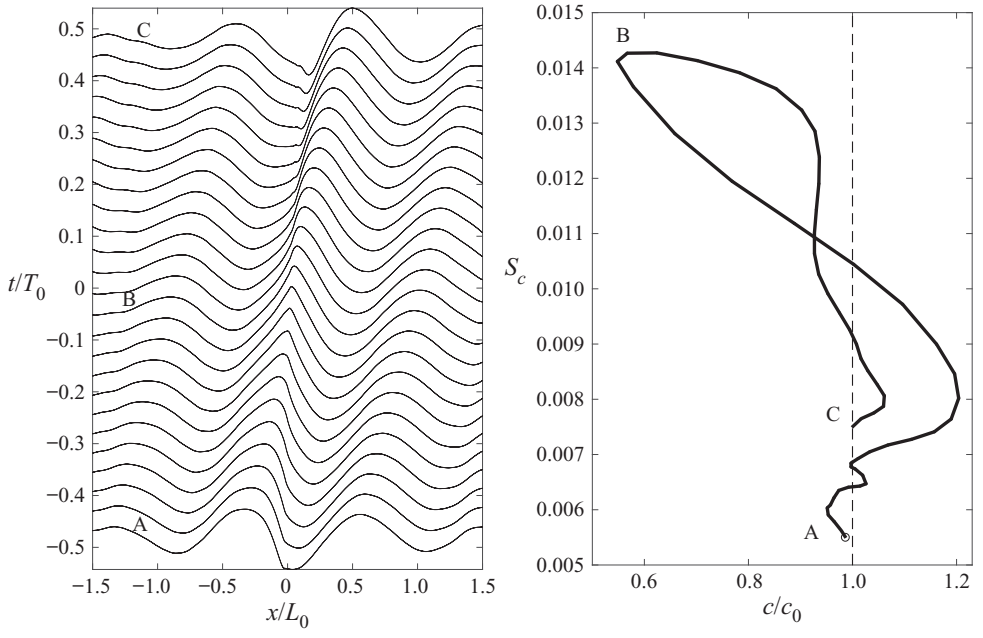


FIGURE 7. Linear crest slowdown of a focusing gravity wave group in deep water (JONSWAP spectrum, spectral bandwidth $\nu = 0.4$, $\Delta = 0.1$). Other symbols are as in caption of figure 2.

effects induced by the dispersive nature of waves. Briefly, a linear unsteady wave group propagates at a speed that includes a dynamical phase velocity dependent on the mean spectral frequency, and an additional geometric phase velocity induced by the changing shape of the crest due to leaning. Fedele (2014*a*) calculates that the leaning coefficient at crest maxima of unsteady oceanic groups attains a slowdown of $c/c_0 \approx 0.8$. Other fluid dynamical phenomena with the same underlying physics include self-propulsion at low Reynolds numbers (Wilczek & Shapere 1989) and the speed of fluctuating coherent structures in turbulent pipe flow that depends on both their dynamical inertia and also on their geometrical shape as it varies in time (Fedele, Abessi & Roberts 2015).

Clearly, the unsteadiness of dispersive focusing is essential for crest slowdown to be observed. The slowdown of a crest is the manifestation of energy flowing through the wave packet: it accumulates in the slowing crest as potential energy, causing the growth in crest amplitude. Then, it is released into kinetic energy as the crest accelerates while reducing its height. However, for waves in deep water, theoretical considerations suggest that third-order nonlinear dispersion tends to speed up the crest, quenching its growth (Fedele 2014*b*). In particular, consider the surface elevation $\eta = \epsilon a_0 B(X, T)\mathrm{e}^{\mathrm{i}(k_0 x - \omega_0 t)}$ of a weakly nonlinear, broadband wave group in deep water. Here, a_0 is the amplitude of the carrier wave at frequency ω_0 and wavenumber k_0, and ϵ is a small parameter to order nonlinearities in terms of spectral bandwidth. Here, the carrier wave is a sinusoidal waveform that is modulated or modified by both linear dispersion and nonlinearities. The dimensionless surface envelope $B(X, T)$ varies on the slow space and time scales $X = \epsilon k_0(x - C_g t)$ and $T = \epsilon^2 \omega_0 t$, where $C_g = c_0/2$ is the group velocity. The envelope satisfies, correct to $O(\epsilon^3)$, the compact Zakharov (cDZ) equation (Dyachenko, Kachulin & Zakharov 2017*a*,*b*) for unidirectional waves, which follows from the general Zakharov equation (Zakharov 1968; Krasitskii 1994; Zakharov 1999). The essential form of the cDZ equation is that of a modified nonlinear Schrödinger (NLS) equation (Fedele & Dutykh

https://doi.org/10.1017/jfm.2020.424 Published online by Cambridge University Press

2012*b*; Fedele 2014*b*,*c*):

$$\mathrm{i}B_T = \frac{1}{8}B_{XX} + \frac{\mathrm{i}\epsilon}{16}B_{XXX} + \underbrace{|B|^2 B}_{NLS} - \underbrace{3\mathrm{i}\epsilon\,|B|^2 B_X}_{Dysthe} - \underbrace{\epsilon^2\,|B|^2 B_{XX}}_{cDZ} + \epsilon^3 N(B), \tag{3.1}$$

where $O(\epsilon^3)$ terms have been collected in $N(B)$ (Fedele & Dutykh 2012*b*). Here, $B_T = \partial_T B$ and $B_X = \partial_X B$ denote the partial derivatives with respect to the slow time and space scales, respectively. The $O(\epsilon^0)$ nonlinear cubic term is that of the NLS equation. The $O(\epsilon)$ nonlinear term is that of the Hamiltonian Dysthe equation (Dysthe 1979; Fedele & Dutykh 2012*a*,*b*) and the new $O(\epsilon^2)$ term is characteristic of the cDZ equation. We note in passing that the original Dysthe (1979) equation is expressed in terms of physical variables, which are non-canonical and the symplectic structure is lost. However, it can be recovered by way of a canonical transformation (Fedele & Dutykh 2012*a*,*b*). All three nonlinear terms tend to reduce the dispersive nature of waves, especially the cDZ term, which is the most effective as the wave envelope B grows in amplitude and broadens in spectral bandwidth during focusing. Indeed, the linear dispersive tendency of the wave packet, as modelled by B_{XX}, mostly reduces by the factor $(1 - 8\epsilon^2|B|^2)$ due to the cDZ term. This term allows for soliton solutions in the form of peakons with discontinuous slope (Fedele & Dutykh 2012*b*). As a result, there is a nonlinear increase in the phase speed $C(k)$ of higher-wavenumber Fourier components, which offsets the linear crest slowdown. To see this, (3.1) is rewritten in the compact differential form

$$\left\{1 - \mathrm{i}\epsilon/2\partial_X + \mathrm{i}\epsilon^2\partial_T - \Omega\left(1 - \mathrm{i}\epsilon\partial_X, \epsilon^2\,|B|^2\right)\right\} B = 0, \tag{3.2}$$

where the associated nonlinear dispersion relation $\Omega(k, |B|^2)$ is given by the Taylor expansion

$$\Omega\left(k, |B|^2\right) = 1 + \frac{K}{2} - \frac{K^2}{8} + \frac{K^3}{16} + |B|^2\left(1 + 3K + K^2\right), \tag{3.3}$$

where $k = 1 + K$, k denotes dimensionless wavenumber (normalized by k_0) and the first four terms represent the third-order Taylor expansion of the deep-water frequency $\sqrt{1+K}$ with respect to K. The nonlinear frequency $\Omega(k, |B|^2)$ increases as the envelope amplitude $|B|$ increases. So does the minimum crest speed in (2.4), where the nonlinear phase speed $C(k) = c_0\Omega(k, |B|^2)/k$ in the integrand increases, leading to larger crest speeds. Thus, the crest slowdown is reduced and the wave growth is suppressed (Fedele 2014*b*; Fedele, Chandre & Farazmand 2016).

The Dysthe term does not suppress the NLS (subharmonic) modulational instability, which is instead affected by the cDZ term. Indeed, modulational instability is suppressed as the wave steepness $\mu = 2|B|$ of the packet increases above 0.27 and breathers are annihilated (Fedele 2014*b*,*c*). Further, the cDZ term induces superharmonic instability as μ exceeds the critical value $\mu_c = 0.577$ and the envelope dynamics change from elliptic (NLS) to hyperbolic type. In particular, Fedele (2014*b*) showed that for $\mu > \mu_c$ a perturbation $\epsilon F(\xi, \tau)$ to the squared envelope $E = |B(X, T)|^2$ evolves according to the hyperbolic modified Korteweg–de Vries equation:

$$F_\tau + \beta F F_\xi + \epsilon\left(z_1 F_{\xi\xi\xi} + z_2 F^2 F_\xi\right) + \epsilon^2 z_3\left(2F_\xi F_{\xi\xi} + F F_{\xi\xi\xi}\right) = 0, \tag{3.4}$$

where $\xi = \epsilon(X - cT)$ and $\tau = \epsilon^2 T$ are independent multiple scales, c is the wave celerity and the coefficients (β, z_j) are given in Fedele (2014*b*). Equation (3.4) typically arises

https://doi.org/10.1017/jfm.2020.424 Published online by Cambridge University Press

in shallow water theory and it describes the tendency of the wave packet to steepen and eventually break in finite time. This suggests possible physical similarities between shallow- and deep-water waves. Fedele (2014*b*) also suggests the transition from elliptic to hyperbolic behaviour in the wave dynamics as the breaking onset, the point of no return beyond which waves inevitably break (Barthelemy *et al.* 2018).

In summary, a key open question discussed in Fedele (2014*a*,*b*) and Fedele *et al.* (2016) is concerned with the effect of wave nonlinearities on the crest slowdown. In the following, we present some theoretical arguments that provide some initial insights, suggesting that nonlinearities have a secondary effect on the magnitude of the leaning and consequently on the slowdown.

3.1. *Nonlinear dispersion effects on the crest slowdown*

We have seen that crest slowdown is a generic feature of linear gravity water wave systems, with relatively large slowdowns ($c/c_0 < 0.7$) obtained in our simulations. In comparison, a more moderate slowdown $c/c_0 \approx 0.8$ was found in our present numerical simulations and in field observations (Banner *et al.* 2014). The reduced slowdown can be explained by accounting for the nonlinear dispersive nature of waves. The slowdown of the largest crest in a wave group reduces because steeper waves are less dispersive at higher wave steepness. In particular, as the wave amplitude increases, shorter elementary waves increase their phase speed, catching up with their longer counterparts. As a result, the nonlinear increase in phase speed offsets the linear crest slowdown due to the finite spectral bandwidth, limiting the slowdown of the wave group. This can be seen from (2.4) for the minimum crest speed, where the phase speed $C(k)$ in the integrand increases, leading to larger crest speeds.

The hypothesis that the reduction of the crest slowdown is due to the nonlinear dispersive nature of waves (Fedele 2014*a*,*b*) is validated by way of recent oceanic space–time field observations using a wave acquisition stereo system (WASS) (see Fedele, Benetazzo & Forristall 2011; Gallego *et al.* 2011; Benetazzo *et al.* 2012; Fedele *et al.* 2013; Gallego *et al.* 2013) and hereafter discussed.

3.2. *Ocean field observations*

A WASS was deployed at the oceanographic tower Acqua Alta in the northern Adriatic Sea, 16 km off the coast of Venice in 16 m depth of water. Stereo video measurements were acquired in three experiments during 2009–2010 to investigate space–time and spectral properties of ocean waves (Fedele *et al.* 2011; Gallego *et al.* 2011; Benetazzo *et al.* 2012; Fedele *et al.* 2013; Gallego *et al.* 2013). To maximize the stereocamera overlap area, the WASS was deployed 12.5 m above the mean sea level at a 70° depression angle. This provided a trapezoidal overlap area with sides of 30 m and 100 m, a width of 100 m and an imaged area of approximately 1100 m^2. We describe results from data acquired during Experiment 2, using 21 000 frames captured at 10 Hz. The mean wind speed was 9.6 m s^{-1} with a 110 km fetch, and the unimodal wave spectrum had a significant wave height $H_s = 1.09$ m and zero-crossing period $T_z = 3.51$ s (Fedele *et al.* 2011, 2013). The observed directional spectrum $S(k, \theta)$ is shown in figure 8. Note the bimodal structure of the spectrum in the high-wavenumber range as observed in oceanic sea states (Banner & Young 1994; Young, Verhagen & Banner 1995; Ewans 1998; Hwang *et al.* 2000; Wang & Hwang 2001; Toffoli *et al.* 2010). Nevertheless, the imaged dominant crests still undergo a slowdown cycle similar to the simulated crests described above.

https://doi.org/10.1017/jfm.2020.424 Published online by Cambridge University Press

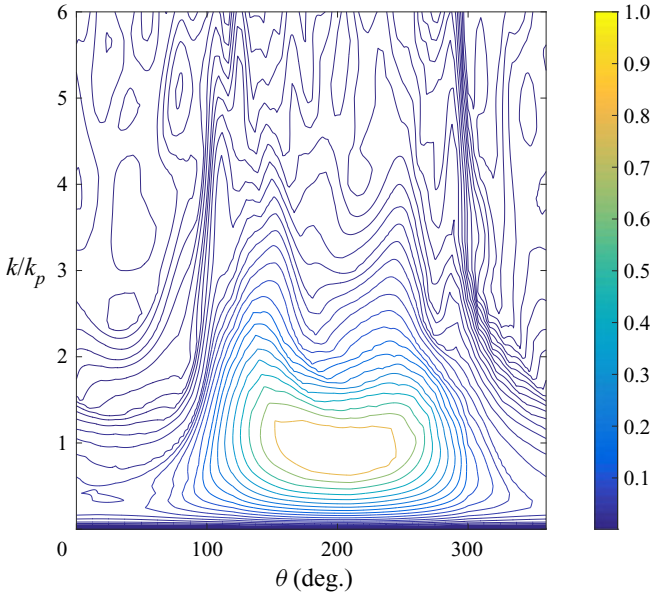


FIGURE 8. The WASS observations at Acqua Alta: observed directional spectrum $S(k, \theta)/S_{max}$ and k_p is the wavenumber at the spectral peak S_{max}.

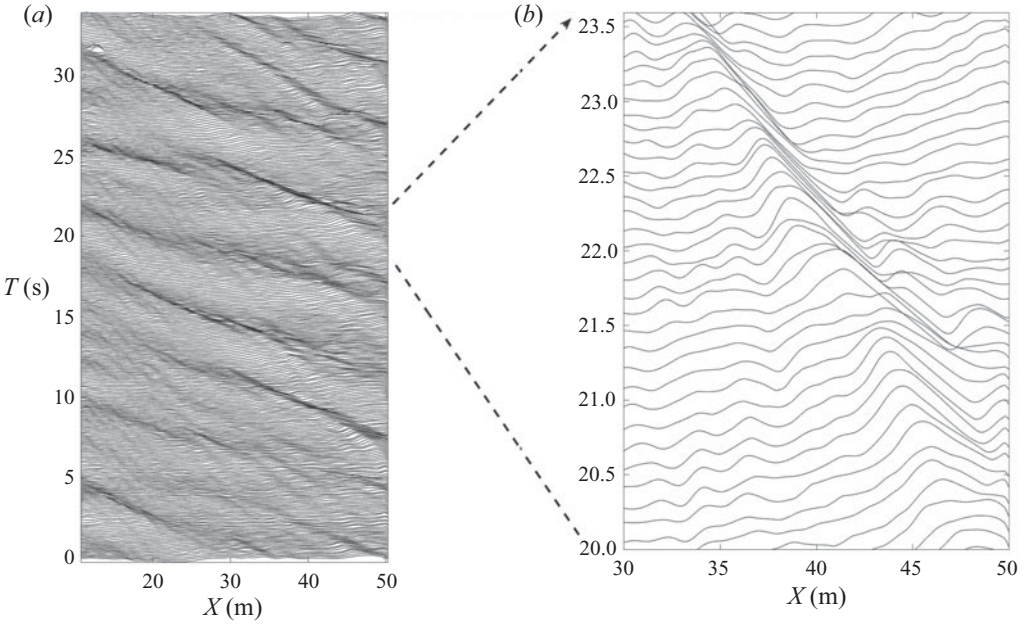


FIGURE 9. The WASS observations at Acqua Alta. (*a*) Time stack of the stereo-observed wave field along the dominant direction (wave profiles stack at the sampling frequency $f_s = 10$ Hz). Waves propagate from left to right; significant wave height $H_s = 1.09$ m and zero-crossing period $T_z = 3.51$ s. (*b*) Details of the leaning cycle of a large crest that leans forward as it slows down before reaching the largest height and then leans backward as it accelerates. Note that the cycle time scale is about T_z.

https://doi.org/10.1017/jfm.2020.424 Published online by Cambridge University Press

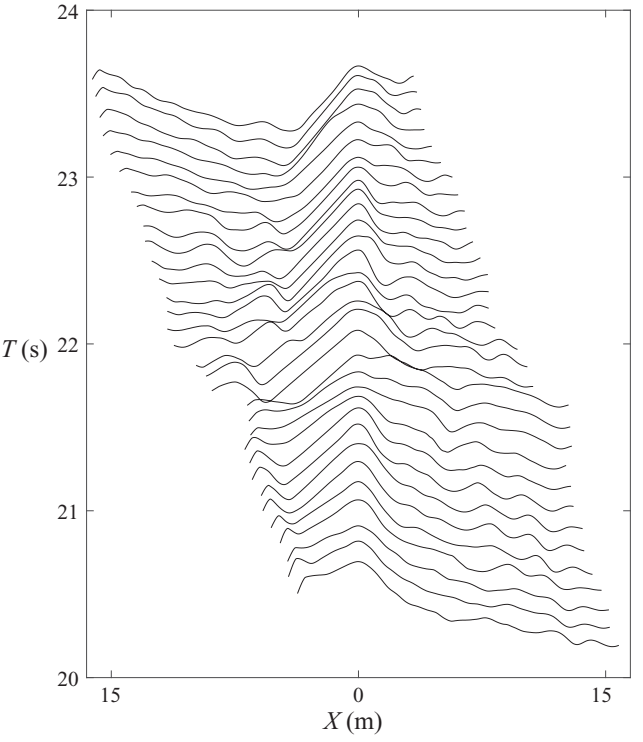


FIGURE 10. The WASS observations at Acqua Alta: leaning cycle of the large crest shown in figure 9 in a reference frame moving with the crest.

Analyses performed include estimating the speed c of focusing crests that travel through the imaged area. Most of the observed crests are very steep and close to breaking. The data were filtered above 1.5 Hz to remove short riding waves. The speeds of crests observed within the imaged area were estimated by tracking the spatial crest along the dominant wave direction. Subpixeling reduced quantization errors in estimating the local crest position. As the imaged area was not large enough to capture a complete focusing event, the local reference wave speed c_0 was calculated using the linear dispersion relationship from the spectral peak frequency of a short time series centred at the crest ($D = 120$ s as an optimal record length) and Doppler-corrected for the in-line 0.20 m s^{-1} mean current. A local wavelength L_c for each crest was estimated as the distance between the two zero-crossings adjacent to the crest. Then, the local crest steepness was estimated as $S_c = k_c a_c$, where $k_c = 2\pi/L_c$ is the local wavenumber and a_c the crest height.

Figure 9(a) shows the space–time evolution of the stereo-reconstructed wave field along the dominant direction. Waves propagate from left to right. In figure 9(b), a detailed evolution of one of the large crests shows that the crest leans forward as it decelerates before reaching the largest height and then it speeds up as it leans backward. This is clearly seen in a frame moving with the crest, as shown in figure 10.

Moreover, the marginal probability density function of the normalized crest speed c by itself estimated from all the measured crests peaks at close to $0.8c_0$, as is clearly seen in figure 11. However, the same speed distribution conditioned on values of wave steepness $S_c > 0.2$ peaks at $0.9c_0$ indicating a reduced slowdown. This is consistent with the nonlinear dispersive nature of waves as discussed above. In the following section, we

https://doi.org/10.1017/jfm.2020.424 Published online by Cambridge University Press

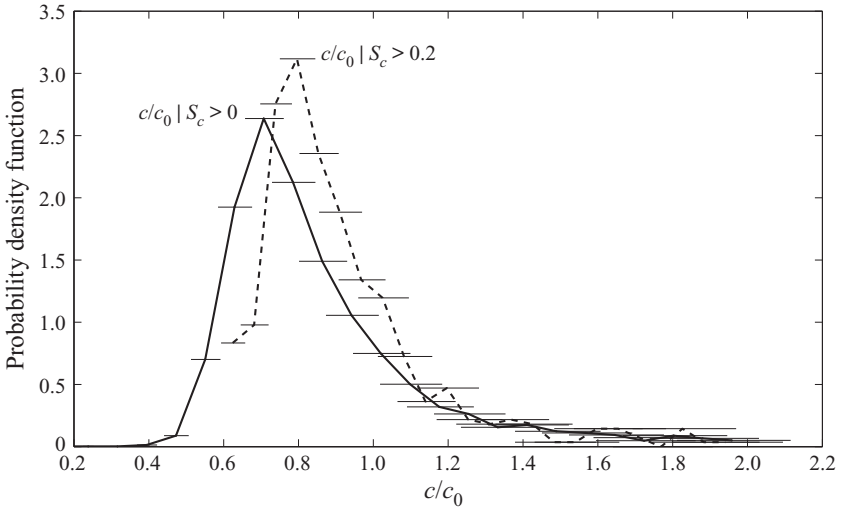


FIGURE 11. The WASS observations at Acqua Alta: (solid line) marginal probability density function of the normalized crest speed c/c_0 and (dashed line) conditioned on crest steepness values $S_c > 0.2$.

show that these ocean observations are also consistent with our numerical simulations of unsteady evolution of unidirectional (2-D) and multidirectional (3-D) dispersive wave packets in both deep and intermediate-depth waters, for a range of wave steepness levels. A reduced slowdown is also observed for waves travelling in intermediate water depth, where waves tend to be less dispersive because of the influence of the ocean bottom.

4. Numerical results

To investigate crest speed slowdown of modulating steep gravity waves, our present study used results from simulations using the boundary element numerical wave tank code WSIM, a 3-D extension of the 2-D code developed by Grilli, Skourup & Svendsen (1989) to solve for single-phase wave motions of a perfect fluid. It has been applied extensively to the solution of finite-amplitude wave propagation and wave breaking problems (see chapter 3 of Ma 2010). The perfect fluid assumption restricts WSIM to simulating breaking impact just prior to surface reconnection of the breaking crest tip to the forward face of the wave. However, its potential theory formulation enables it to simulate wave propagation in a CPU-efficient way, without the diffusion issues of viscous numerical codes. The simulation of wave generation and development of the onset of breaking events can be carried out with great precision (e.g. Fochesato & Dias 2006; Fochesato, Grilli & Dias 2007). The WSIM code has been validated extensively for wave evolution in deep and intermediate-depth water and shows excellent energy conservation (Grilli *et al.* 1989; Grilli & Svendsen 1990; Grilli & Subramanya 1994, 1996; Grilli & Horrillo 1997; Grilli, Guyenne & Dias 2001; Fochesato & Dias 2006; Fochesato *et al.* 2007).

With reference to table 1 of Barthelemy *et al.* (2018), we consider a suite of representative 2-D and 3-D gravity wave groups in deep and transitional waters. From the simulated wave profiles, we computed the evolution of the crest velocity c as a function of the local crest steepness $S_c = k_c a_c$, where a_c is the amplitude of the crest and

https://doi.org/10.1017/jfm.2020.424 Published online by Cambridge University Press

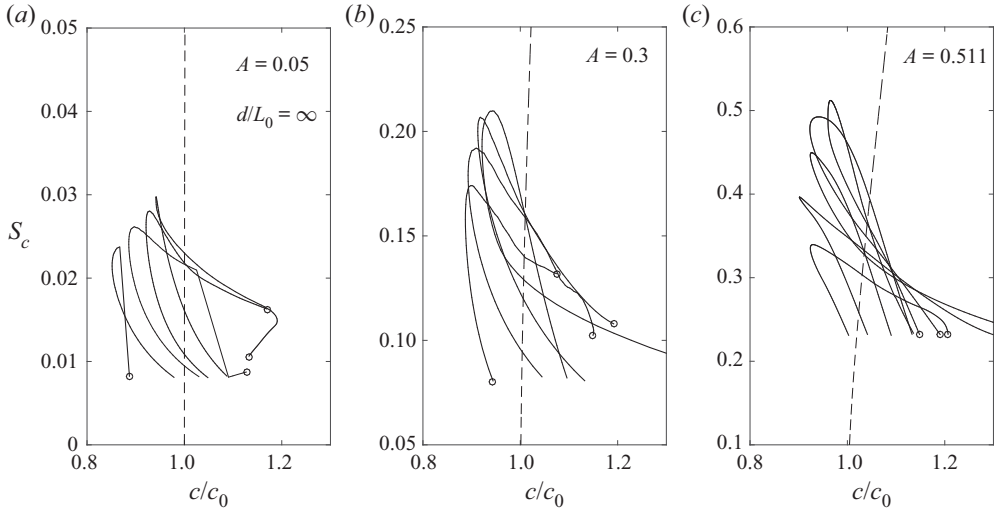


FIGURE 12. Hysteresis diagrams S_c against c/c_0 for 2-D deep-water C3N5 small steepness (*a*), moderate steepness (*b*) and maximally steep non-breaking (*c*) gravity wave groups. Here, c_0 is the reference linear deep-water phase speed of the dominant frequency ω_0. Dashed lines depict fifth-order Stokes prediction (Fenton 1979, 1985).

$k_c = 2\pi/L_c$ is the associated local wavenumber, with L_c being the distance between the two zero-crossings adjacent to the crest. In each simulated case, the crest velocity c has been normalized by the linear phase speed c_0. For reference, we consider the celerity c in (1.1) of a fifth-order Stokes steady wave and the associated local steepness S_c is computed from the theoretical profiles (Fenton 1979, 1985). Three different methods (local, average and global) were used to obtain $c_0 = \omega_0/k_0$. The linear velocity c_0 is computed without assuming a dispersion relationship, using the spectral-peak frequency ω_0 at the wavenumber k_0. The local method values were found by computing k_0 from the spatial fast Fourier transform (FFT) at an arbitrary time and ω_0 from a FFT time series centred on the position of the peak of the wave group at this given time. The average method determined ω_0 from the ensemble mean FFT of the time series from 15 virtual height probes spaced uniformly between two crest (or trough) maxima. Wavenumber k_0 was determined from the ensemble mean FFT of 512 surface profiles between two crest (or trough) maxima. The global method used a 2-D FFT over the entire space–time domain of the simulation to obtain the dispersion graph from which ω_0 and k_0 were extracted. Refined values were found using an interpolating polynomial around the power spectral maxima. We observed that the values of c_0 obtained from the average and the global methods agree within ± 1 %.

With reference to table 1 of Barthelemy *et al.* (2018), consider the simulated 2-D C3N5 wave packets in deep water. Figure 12 shows hysteresis diagrams S_c against c/c_0 for C3N5 small (figure 12*a*) and moderate (figure 12*b*) steepness, as well as maximally steep non-breaking (figure 12*c*) gravity wave groups. Here, c_0 is the reference linear deep-water phase speed of the dominant frequency ω_0. In particular, figure 12(*a*) depicts the same hysteresis diagram of a 2-D C3N5 deep-water gravity wave packet with small steepness ($A = 0.05$). Figure 12(*b*) shows the hysteresis diagram for the same group with moderate steepness ($A = 0.3$), whereas the maximum non-breaking state ($A = 0.511$) is shown in figure 12(*c*). Here, A is the maximum local steepness S_c observed in the wave

https://doi.org/10.1017/jfm.2020.424 Published online by Cambridge University Press

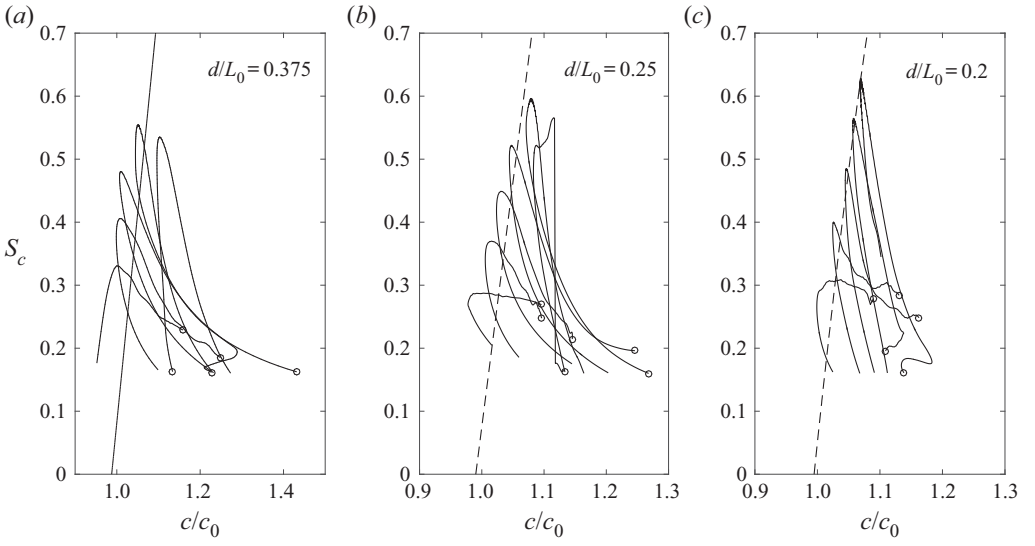


FIGURE 13. Hysteresis diagrams S_c against c/c_0 for 2-D D3N9 gravity wave groups from deep to transitional waters. Here, c_0 is the reference linear finite-depth phase speed of the dominant frequency ω_0. Dashed lines depict fifth-order Stokes prediction (Fenton 1979, 1985).

group simulation. The prediction of crest velocity dependence on steepness based on fifth-order Stokes theory (Fenton 1979, 1985) is shown by the dashed line. The crest velocities for the small-steepness wave group have the largest range varying in the interval $[0.85c_0–1.2c_0]$. As the steepness increases, this dynamical range reduces especially for the highly nonlinear maximum non-breaking case (figure 12*c*), where the minimum crest velocities cluster more closely around $0.9c_0$.

Two important findings for this generic class of wave packets are apparent. First, all the crests of the wave group experience a crest velocity slowdown. Second, in each wave group case there is a tendency for the minimum speed of the ensemble of crests to increase as the local steepness increases. The slowdown experienced by all the crests within a wave group is dependent on the steepness of the group and the leaning cycles have almost the same duration close to the dominant wave period, irrespective of the group length. This is expected as waves in a group are phase-locked. In particular, for the small-steepness 2-D wave group (see figure 12*a*) both small and large crests experience a comparable crest slowdown, indicating that the slowdown is practically insensitive to the degree of phase coherence/focus of each crest. In contrast, crests of the maximally non-breaking wave group (see figure 12*c*) experience a slowdown that is smaller for steeper crests. In each panel, the hysteresis curves tend to bend upward as the maximum crest steepness increases, with a reduction in the associated crest speed slowdown and smaller dynamical ranges of crest speeds.

In summary, figure 12 shows that crests of deep-water gravity wave groups have a complex evolution, slowing down towards a similar minimum value. No major differences in the hysteresis curves between 2-D and strongly converging 3-D gravity wave groups are seen, leading to the important conclusion that crest slowdown behaviour is a generic feature of 2-D and 3-D unsteady gravity wave packets as discussed below. Even at lower steepness levels, similar patterns in crest slowdown are observed. Moreover, the slowdown of crests within steep gravity wave groups reduces as the local steepness increases,

https://doi.org/10.1017/jfm.2020.424 Published online by Cambridge University Press

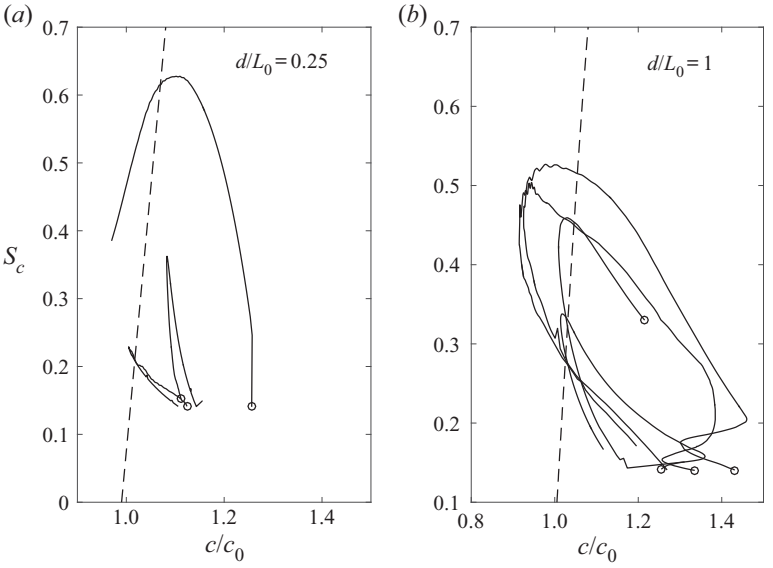


FIGURE 14. Hysteresis diagrams S_c against c/c_0 for 3-D C3N9 gravity wave groups in transitional water (*a*) and in deep water (*b*). Here, c_0 is the reference linear finite-depth phase speed of the dominant frequency ω_0. Dashed lines depict fifth-order Stokes prediction (Fenton 1979, 1985).

suggesting that nonlinear dispersion is a plausible mechanism for the slowdown reduction. In brief, crest slowdown reduces when waves steepen as they become less dispersive.

Gravity waves also become less dispersive when they propagate over water of finite depth, and the crest slowdown is reduced. This is clearly seen in figure 13, which shows the hysteresis diagrams S_c versus c/c_0 of crests of a 2-D D3N9 gravity wave packet from intermediate ($d/L_0 = 0.375$; figure 13*a*) to relatively shallow water depths ($d/L_0 = 0.25$ and 0.2; figure 13*b*,*c*). Clearly, steeper crests experience a reduced dynamical range of values with smaller slowdown that decreases as the water depth reduces, that is, the hysteresis curves bend upward as water depth reduces. As a result, the associated crest speed slowdown reduces and the crest speeds tend to align with the predicted fifth-order Stokes phase speed predictions (Fenton 1979, 1985) (dashed lines), especially as the maximum crest steepness increases.

Representative short-crested (3-D) wave packets also exhibit similar crest slowdown hysteresis curve behaviour, including the abatement of the slowdown effect when the waves travel in shallower water. This is seen in figure 14, which depicts results from model simulations of strongly laterally convergent C3N9 (X10) wave packets with $d/L_0 = 0.25$ (figure 14*a*) and $d/L_0 = 1$ (figure 14*b*) (see table 2 of Barthelemy *et al.* (2018)).

These results support our hypothesis that reduced slowdown of steep crests is due to the nonlinear nature of gravity surface waves, which tend to be less dispersive either when their steepness increases or when they travel from deep water to shallow water.

5. Conclusions

This study provides new insights into the geometric and kinematic properties of the generic crest slowdown of linear and highly nonlinear unsteady gravity wave groups. This phenomenon is essentially due to the dispersive nature of surface waves. Crest slowdown

https://doi.org/10.1017/jfm.2020.424 Published online by Cambridge University Press

is observed routinely for linear (small-steepness) gravity wave groups. It is enhanced as the spectral bandwidth increases, but it is essentially insensitive to the degree of phase coherence and focusing within a wave group. Further, the analysis of the kinematics of both simulated and observed ocean waves reveals a forward-to-backward leaning cycle for the individual wave crests within a wave group, leading to a systematic local crest slowdown of 15–20 % of the reference wave velocity. Stereo ocean observations show that the crest slowdown reduces as the wave steepness increases. This is consistent with our hypothesis that the slowdown of steep crests is reduced because gravity surface waves tend to be less dispersive at higher steepness, or as they propagate over water of intermediate depth. This is supported by numerical simulations of unsteady evolution of 2-D and 3-D dispersive wave packets in both deep and intermediate waters. While our major focus is on gravity waves where generic crest slowdown occurs, results for capillary-dominated waves are also discussed, for which crest speeds cyclically speed up. Overall, these findings contribute new insight into how water-wave groups propagate when the constraint of steadiness is relaxed, providing the unsteady basic state for the onset of breaking or maximally steep non-breaking waves in 2-D and 3-D gravity wave packets. In the context of wave breaking onset in deep and intermediate-depth water, we note that the observed significantly reduced speed of initiation of breaker fronts reported from time to time in the literature (Banner *et al.* 2014) is explained by the crest slowdown properties described in this paper. This aspect has been investigated in detail in our companion paper which proposes a generic new threshold for predicting breaking onset (Barthelemy *et al.* 2018).

Acknowledgments

The WASS deployment at Acqua Alta was supported by CASE-EJ1P Joint Industry Project (no. 4545093). The analysis of video measurements was also supported by ONR grant BAA 09-012: ‘Ocean Wave Dissipation and Energy Balance (WAVE-DB): toward reliable spectra and first breaking statistics’. M.L.B. and X.B. were supported by the Australian Research Council under Discovery Projects DP0985602 and DP120101701.

Declaration of interests

The authors report no conflict of interest.

Appendix A

Consider N Fourier modes at $k_j = j\Delta k$ separated by Δk of $O(1/N)$. Then the wave surface displacements in (2.1) can be written as the Riemann sum

$$\zeta(\alpha, N) = \sum_{j=1}^{N} a_j \cos(k_j x - \omega_j t + \alpha\theta_j), \tag{A 1}$$

where $\omega_j = \omega(k_j)$ and the Fourier amplitude $a_j = S_n(k_j)\Delta k$ is of $O(1/N)$. The sum $\sum a_j$ of the N amplitudes is finite and of $O(1)$ and the sum $\sum a_j^2$ of the squared amplitudes is of $O(1/N)$. Note that ζ in (2.1) differs from the classical definition of a Gaussian sea just by the definition of the Fourier amplitudes a_j. For Gaussian displacements, $a_j = \sqrt{2S_n(k_j)\Delta k}$, and a_j is of $O(1/\sqrt{N})$.

https://doi.org/10.1017/jfm.2020.424 Published online by Cambridge University Press

That said,

$$\zeta(\alpha, N) = \sum_{j=1}^{N} a_j \left[\cos(k_j x - \omega_j t)\beta_j - \sin(k_j x - \omega_j t)\gamma_j\right], \tag{A 2}$$

where we have defined the random variables

$$\beta_j = \cos(\alpha\theta_j), \quad \gamma_j = \sin(\alpha\theta_j). \tag{A 3a,b}$$

The mean and variance of β_j are

$$\mu_{\beta_j} = \frac{\sin(\pi\alpha)}{\pi\alpha}, \quad \sigma^2_{\beta_j} = \frac{1}{2} + \frac{\sin(2\pi\alpha)}{4\pi\alpha} - \left(\frac{\sin(\pi\alpha)}{\pi\alpha}\right)^2, \tag{A 4a,b}$$

and

$$\mu_{\gamma_j} = 0, \quad \sigma^2_{\gamma_j} = \frac{1}{2} - \frac{\sin(2\pi\alpha)}{4\pi\alpha}, \tag{A 5a,b}$$

for any integers j. Then, the mean and variance of η follow as

$$\mu_\zeta(\alpha, N) = \sum_{j=1}^{N} a_j \frac{\sin(\pi\alpha)}{\pi\alpha} \cos(k_j x - \omega_j t) \tag{A 6}$$

and

$$\sigma^2_\zeta(\alpha, N) = \frac{1}{2}\sum_{j=1}^{N} a_j^2 \left[1 + \cos(2k_j x - 2\omega_j t)\frac{\sin(2\pi\alpha)}{2\pi\alpha} - 2\cos(k_j x - \omega_j t)^2 \left(\frac{\sin(\pi\alpha)}{\pi\alpha}\right)^2\right]. \tag{A 7}$$

Note that $\int S_n(k)\,\mathrm{d}k = 1$. Then, $\sum_{j=1}^{N} a_j \to 1$ in the limit of $N \to \infty$, since a_j are of $O(1/N)$. Further, the sum of the squared amplitudes $\sum_{j=1}^{N} a_j^2 \to 0$ because the sum of N terms of $O(1/N^2)$ is infinitesimally small as $N \to \infty$. In the same limit, the variance σ^2_η vanishes and η tends, with probability 1, to its expected value

$$\zeta = \lim_{N\to\infty} \mu_\eta(\alpha, N) = \sum_{j=1}^{N} a_j \frac{\sin(\pi\alpha)}{\pi\alpha} \cos(k_j x - \omega_j t), \tag{A 8}$$

as a consequence of the strong law of large numbers (Latifah & van Groesen 2012). This has been confirmed by way of Monte Carlo simulations. In particular, we observed that convergence is practically attained when we use a number of Fourier modes $N > 10^4$ to synthesize the wave group, and variability around the mean is observed for number of Fourier modes less than N. In integral form,

$$\zeta(x, t; \alpha) = \widetilde{h}(\alpha) \int S_n(k) \cos(kx - \omega t)\,\mathrm{d}k, \tag{A 9}$$

which is identical to the perfectly focusing group ζ in (2.1) except that now the crest amplitude is given by

$$\widetilde{h}(\alpha) = h\frac{\sin(\pi\alpha)}{\pi\alpha}, \tag{A 10}$$

and it is smaller than the maximal height $h = \widetilde{h}(\alpha = 0)$ when the focus of the wave packet is perfect.

https://doi.org/10.1017/jfm.2020.424 Published online by Cambridge University Press

REFERENCES

BALDOCK, T. E., SWAN, C. & TAYLOR, P. H. 1996 A laboratory study of nonlinear surface waves on water. *Phil. Trans.* **354** (1707), 649–676.

BANNER, M. L., BARTHELEMY, X., FEDELE, F., ALLIS, M., BENETAZZO, A., DIAS, F. & PEIRSON, W. L. 2014 Linking reduced breaking crest speeds to unsteady nonlinear water wave group behavior. *Phys. Rev. Lett.* **112**, 114502.

BANNER, M. L. & PEIRSON, W. L. 2007 Wave breaking onset and strength for two-dimensional deep-water wave groups. *J. Fluid Mech.* **585**, 93–115.

BANNER, M. L. & YOUNG, I. R. 1994 Modeling spectral dissipation in the evolution of wind waves. Part I: assessment of existing model performance. *J. Phys. Oceanogr.* **24** (7), 1550–1571.

BARTHELEMY, X., BANNER, M. L., PEIRSON, W. L., FEDELE, F., ALLIS, M. & DIAS, F. 2018 On a unified breaking onset threshold for gravity waves in deep and intermediate depth water. *J. Fluid Mech.* **841**, 463–488.

BENETAZZO, A., FEDELE, F., GALLEGO, G., SHIH, P.-C. & YEZZI, A. 2012 Offshore stereo measurements of gravity waves. *Coastal Engng* **64**, 127–138.

BERRY, M. 1988 The geometric phase. *Sci. Am.* **259** (6), 46–52.

BEYÁ, J. F., PEIRSON, W. L. & BANNER, M. L. 2012 Turbulence beneath finite amplitude water waves. *Exp. Fluids* **52**, 1319–1330.

BOCCOTTI, P. 2000 *Wave Mechanics for Ocean Engineering*. Elsevier Sciences.

CRACIUNESCU, C. C. & CHRISTOU, M. 2019*a* The effect of wave crest speed in breaking waves. *IOP Conf. Ser.* **586**, 012039.

CRACIUNESCU, C. C. & CHRISTOU, M. 2019*b* Identifying breaking waves from measured time traces. In *The 29th International Ocean and Polar Engineering Conference, 16–21 June, Honolulu, Hawaii, USA*. International Society of Offshore and Polar Engineers.

DYACHENKO, A. I., KACHULIN, D. I. & ZAKHAROV, V. E. 2017*a* Envelope equation for water waves. *J. Ocean Engng Marine Energy* **3**, 409–415.

DYACHENKO, A. I., KACHULIN, D. I. & ZAKHAROV, V. E. 2017*b* Super compact equation for water waves. *J. Fluid Mech.* **828**, 661–679.

DYSTHE, K. B. 1979 Note on a modification to the nonlinear schrodinger equation for application to deep water waves. *Proc. R. Soc. Lond.* A **369** (1736), 105–114.

EWANS, K. C. 1998 Observations of the directional spectrum of fetch-limited waves. *J. Phys. Oceanogr.* **28** (3), 495–512.

FEDELE, F. 2008 Rogue waves in oceanic turbulence. *Physica D* **237** (14–17), 2127–2131.

FEDELE, F. 2014*a* Geometric phases of water waves. *Europhys. Lett.* **107** (6), 69001.

FEDELE, F. 2014*b* On certain properties of the compact Zakharov equation. *J. Fluid Mech.* **748**, 692–711.

FEDELE, F. 2014*c* On the persistence of breathers at deep water. *J. Expl. Theor. Phys. Lett.* **98** (9), 523–527.

FEDELE, F. 2015 On the kurtosis of ocean waves in deep water. *J. Fluid Mech.* **782**, 25–36.

FEDELE, F., ABESSI, O. & ROBERTS, P. J. 2015 Symmetry reduction of turbulent pipe flows. *J. Fluid Mech.* **779**, 390–410.

FEDELE, F., BENETAZZO, A. & FORRISTALL, G. Z. 2011 Space-time waves and spectra in the Northern Adriatic Sea via a wave acquisition stereo system. In *Proceedings of the ASME 2011 30th International Conference on Offshore Mechanics and Arctic Engineering*, vol. 2, pp. 651–663.

FEDELE, F., BENETAZZO, A., GALLEGO, G., SHIH, P.-C., YEZZI, A., BARBARIOL, F. & ARDHUIN, F. 2013 Space-time measurements of oceanic sea states. *Ocean Model.* **70**, 103–115.

FEDELE, F., CHANDRE, C. & FARAZMAND, M. 2016 Kinematics of fluid particles on the sea surface: Hamiltonian theory. *J. Fluid Mech.* **801**, 260–288.

FEDELE, F. & DUTYKH, D. 2012*a* Hamiltonian form and solitary waves of the spatial dysthe equations. *J. Expl. Theor. Phys. Lett.* **94** (12), 840–844.

FEDELE, F. & DUTYKH, D. 2012*b* Special solutions to a compact equation for deep-water gravity waves. *J. Fluid Mech.* **712**, 646–660.

FEDELE, F. & TAYFUN, M. A. 2009 On nonlinear wave groups and crest statistics. *J. Fluid Mech.* **620**, 221–239.

FENTON, J. 1985 A fifth-order Stokes theory for steady waves. *J. Waterway Port Coastal Ocean Engng* **111** (2), 216–234.

https://doi.org/10.1017/jfm.2020.424 Published online by Cambridge University Press

FENTON, J. D. 1979 A high-order cnoidal wave theory. *J. Fluid Mech.* **94**, 129–161.

FOCHESATO, C. & DIAS, F. 2006 A fast method for nonlinear three-dimensional free-surface waves. *Proc. R. Soc.* A **462** (2073), 2715–2735.

FOCHESATO, C., GRILLI, S. & DIAS, F. 2007 Numerical modeling of extreme rogue waves generated by directional energy focusing. *Wave Motion* **44** (5), 395–416.

GALLEGO, G., YEZZI, A., FEDELE, F. & BENETAZZO, B. 2011 A variational stereo method for the three-dimensional reconstruction of ocean waves. *IEEE Trans. Geosci. Remote Sens.* **49** (11), 4445–4457.

GALLEGO, G., YEZZI, A., FEDELE, F. & BENETAZZO, B. 2013 Variational stereo imaging of oceanic waves with statistical constraints. *IEEE Trans. Image Process.* **22** (11), 4211–4223.

GEMMRICH, J. R., BANNER, M. L. & GARRETT, C. 2008 Spectrally resolved energy dissipation rate and momentum flux of breaking waves. *J. Phys. Oceanogr.* **38** (6), 1296–1312.

GRILLI, S. T., GUYENNE, P. & DIAS, F. 2001 A fully non-linear model for three-dimensional overturning waves over an arbitrary bottom. *Intl. J. Numer. Methods Fluids* **35** (7), 829–867.

GRILLI, S. T. & HORRILLO, J. 1997 Numerical generation and absorption of fully nonlinear periodic waves. *J. Engng Mech.* **123** (10), 1060–1069.

GRILLI, S. T., SKOURUP, J. & SVENDSEN, I. A. 1989 An efficient boundary element method for nonlinear water waves. *Engng Anal. Bound. Elem.* **6** (2), 97–107.

GRILLI, S. T. & SUBRAMANYA, R. 1994 Quasi-singular integrals in the modeling of nonlinear water waves in shallow water. *Engng Anal. Bound. Elem.* **13** (2), 181–191.

GRILLI, S. T. & SUBRAMANYA, R. 1996 Numerical modeling of wave breaking induced by fixed or moving boundaries. *Comput. Mech.* **17** (6), 374–391.

GRILLI, S. T. & SVENDSEN, I. A. 1990 Corner problems and global accuracy in the boundary element solution of nonlinear wave flows. *Engng Anal. Bound. Elem.* **7** (4), 178–195.

GRUE, J., CLAMOND, D., HUSEBY, M. & JENSEN, A. 2003 Kinematics of extreme waves in deep water. *Appl. Ocean Res.* **25** (6), 355–366.

HASSELMANN, K., BARNETT, T. P., BOUWS, E, CARLSON, H, CARTWRIGHT, D. E., ENKE, K, EWING, J. A., GIENAPP, H, HASSELMANN, D. E., KRUSEMAN, P. *et al.*1973 Measurements of wind-wave growth and swell decay during the Joint North Sea Wave Project (JONSWAP). *Ergänzungshef*, **8** (12).

HWANG, P. A., WANG, D. W., WALSH, E. J., KRABILL, W. B. & SWIFT, R. N. 2000 Airborne measurements of the wavenumber spectra of ocean surface waves. Part II: directional distribution. *J. Phys. Oceanogr.* **30** (11), 2768–2787.

ITAY, U. & LIBERZON, D. 2017 Lagrangian kinematic criterion for the breaking of shoaling waves. *J. Phys. Oceanogr.* **47** (4), 827–833.

JESSUP, A. T. & PHADNIS, K. R. 2005 Measurement of the geometric and kinematic properties of microscale breaking waves from infrared imagery using a PIV algorithm. *Meas. Sci. Technol.* **16** (10), 1961.

JOHANNESSEN, T. B. 2010 Calculations of kinematics underneath measured time histories of steep water waves. *Appl. Ocean Res.* **32** (4), 391–403.

JOHANNESSEN, T. B. & SWAN, C. 2001 A laboratory study of the focusing of transient and directionally spread surface water waves. *Proc. R. Soc. Lond.* A **457** (2008), 971–1006.

JOHANNESSEN, T. B. & SWAN, C. 2003 On the nonlinear dynamics of wave groups produced by the focusing of surface-water waves. *Proc. R. Soc. Lond.* A **459** (2032), 1021–1052.

KATSARDI, V. & SWAN, C. 2011 The evolution of large non-breaking waves in intermediate and shallow water. I. Numerical calculations of uni-directional seas. *Proc. R. Soc. Lond.* A **467** (2127), 778–805.

KHAIT, A. & SHEMER, L. 2018 On the kinematic criterion for the inception of breaking in surface gravity waves: fully nonlinear numerical simulations and experimental verification. *Phys. Fluids* **30** (5), 057103.

KINSMAN, B. 1965 *Wind Waves: Their Generation and Propagation on the Ocean Surface*. Prentice-Hall.

KLEISS, J. M. & MELVILLE, W. K. 2010 Observations of wave breaking kinematics in fetch-limited seas. *J. Phys. Oceanogr.* **40** (12), 2575–2604.

KOMEN, G. J. 1994 *Dynamics and Modelling of Ocean Waves*. Cambridge University Press.

KRASITSKII, V. P. 1994 On reduced equations in the Hamiltonian theory of weakly nonlinear surface waves. *J. Fluid Mech.* **272**, 1–20.

https://doi.org/10.1017/jfm.2020.424 Published online by Cambridge University Press

LATIFAH, A. L. & VAN GROESEN, E. 2012 Coherence and predictability of extreme events in irregular waves. *Nonlinear Process. Geophys.* **19** (2), 199–213.

LIBERZON, D. & SHEMER, L. 2011 Experimental study of the initial stages of wind waves' spatial evolution. *J. Fluid Mech.* **681**, 462–498.

LONGUET-HIGGINS, M. S. 1957 On the velocities of the maxima in a moving wave-form. *Math. Proc. Camb. Phil. Soc.* **53** (01), 230–233.

LONGUET-HIGGINS, M. S. 1987 The propagation of short surface waves on longer gravity waves. *J. Fluid Mech.* **177**, 293–306.

LONGUET-HIGGINS, M. S. & STEWART, R. W. 1960 Changes in the form of short gravity waves on long waves and tidal currents. *J. Fluid Mech.* **8**, 565–583.

MA, Q. 2010 *Advances in Numerical Simulation of Nonlinear Water Waves*. World Scientific.

MELVILLE, W. K. 1983 Wave modulation and breakdown. *J. Fluid Mech.* **128**, 489–506.

MELVILLE, W. K. & MATUSOV, P. 2002 Distribution of breaking waves at the ocean surface. *Nature* **417** (6884), 58–63.

MELVILLE, W. K., VERON, F. & WHITE, C. J. 2002 The velocity field under breaking waves: coherent structures and turbulence. *J. Fluid Mech.* **454**, 203–233.

MILLER, S. J., SHEMDIN, O. H. & LONGUET-HIGGINS, M. S. 1991 Laboratory measurements of modulation of short-wave slopes by long surface waves. *J. Fluid Mech.* **233**, 389–404.

PHILLIPS, O. M. 1985 Spectral and statistical properties of the equilibrium range in wind-generated gravity waves. *J. Fluid Mech.* **156**, 505–531.

RAPP, R. J. & MELVILLE, W. K. 1990 Laboratory measurements of deep-water breaking waves. *Phil. Trans. R. Soc. Lond.* A **331** (1622), 735–800.

SHEMER, L. 2013 On kinematics of very steep waves. *Nat. Hazards Earth Syst. Sci.* **13** (8), 2101–2107.

SHEMER, L. & EE, B. K. 2015 Steep unidirectional wave groups – fully nonlinear simulations vs. experiments. *Nonlinear Process. Geophys.* **22** (6), 737–747.

SHEMER, L. & LIBERZON, D. 2014 Lagrangian kinematics of steep waves up to the inception of a spilling breaker. *Phys. Fluids* **26** (1), 016601.

SONG, J.-B. & BANNER, M. L. 2002 On determining the onset and strength of breaking for deep water waves. Part I: unforced irrotational wave groups. *J. Phys. Oceanogr.* **32** (9), 2541–2558.

STANSELL, P. & MACFARLANE, C. 2002 Experimental investigation of wave breaking criteria based on wave phase speeds. *J. Phys. Oceanogr.* **32** (5), 1269–1283.

STOKES, G. G. 1847 On the theory of oscillatory waves. *Trans. Camb. Phil. Soc.* **8**, 441–455.

SULLIVAN, P. P., BANNER, M. L., MORISON, R. P. & PEIRSON, W. L. 2018 Turbulent flow over steep steady and unsteady waves under strong wind forcing. *J. Phys. Oceanogr.* **48** (1), 3–27.

SUTHERLAND, J., GREATED, C. A. & EASSON, W. J. 1995 Variations in the crest kinematics of wave groups. *Appl. Ocean Res.* **17** (1), 55–62.

TAYFUN, M. A. 1986 On narrow-band representation of ocean waves: 1. Theory. *J. Geophys. Res.* **91** (C6), 7743–7752.

TOFFOLI, A., ONORATO, M., BITNER-GREGERSEN, E. M. & MONBALIU, J. 2010 Development of a bimodal structure in ocean wave spectra. *J. Geophys. Res.* **115**, C03006.

VIOTTI, C., CARBONE, F. & DIAS, F. 2014 Conditions for extreme wave runup on a vertical barrier by nonlinear dispersion. *J. Fluid Mech.* **748**, 768–788.

WANG, D. W. & HWANG, P. A. 2001 Evolution of the bimodal directional distribution of ocean waves. *J. Phys. Oceanogr.* **31** (5), 1200–1221.

WIEGEL, R. L. 1964 *Oceanographical Engineering*. Prentice-Hall.

WILCZEK, F. & SHAPERE, A. (Ed.) 1989 *Geometric Phases in Physics*, Advanced Series in Mathematical Physics, vol. 5. World Scientific.

YOUNG, I. R., VERHAGEN, L. A. & BANNER, M. L. 1995 A note on the bimodal directional spreading of fetch-limited wind waves. *J. Geophys. Res.* **100** (C1), 773–778.

ZAKHAROV, V. E. 1968 Stability of periodic waves of finite amplitude on the surface of a deep fluid. *Sov. Phys. J. Appl. Mech. Tech. Phys.* **4**, 190–194.

ZAKHAROV, V. E. 1999 Statistical theory of gravity and capillary waves on the surface of a finite-depth fluid. *Eur. J. Mech. B/Fluids* **18** (3), 327–344.

https://doi.org/10.1017/jfm.2020.424 Published online by Cambridge University Press